

A Thermodynamic Model to Calculate Burning Speed of Methane-Air- Diluent Mixtures

Faranak Rahim, Kian Eisazadeh Far, Farzan Parsinejad,
Raymond J. Andrews and Hameed Metghalchi*

Mechanical and Industrial Engineering Department
Northeastern University
Boston, Massachusetts 02115, USA
Email: metghalchi@coe.neu.edu

Abstract

A thermodynamic model to calculate burning speed of methane-air-diluent mixtures from the measured dynamic pressure rise of a combustion process in a chamber has been developed. The effect of automotive exhaust gas on the burning speeds was measured using a mixture of 86 % N₂ and 14 % CO₂ as the diluent. Photographic observations were made through the end windows in the cylindrical chamber using a high-speed charged coupled device (CCD) camera with variable speed of up to 8000 frames/second. The measured values of burning speeds have been compared with laminar burning speeds calculated using the PREMIX flame speed code and the GRI-Mech 3.0 mechanism. This thermodynamic model is valid for a wide range of high temperatures and pressures and the results agree well with the measurements under these conditions when the flames are smooth or cracked and lean or stoichiometric.

Keywords: Burning speed, constant volume chamber, thermodynamic model

1. Introduction

The purpose of this paper is to present a thermodynamic model for burning speed calculation of methane-oxidizer-diluent mixtures. Laminar burning speed data is important both for developing and testing fluid dynamics and chemical kinetic models of hydrocarbon oxidation and for a wide range of direct practical applications in the fields of engines, burners, explosions, and chemical processors.

Over the past several decades, a great deal of experimental (Davis et al. 1998 and Hunter et al. 1994) and theoretical (Habik et al. 1994 and Wartatz 1984) work has been done on the measurement and kinetic modeling of laminar burning speeds. This has led to the development of fairly complete and reliable flame speed codes and chemical kinetic models for predicting the laminar burning speeds of simple hydrocarbon mixtures at high temperatures and low pressures. Some of the released models involve chemical kinetics modeling, which complicates computations. In addition, relatively little effort has been devoted to measuring or developing models of laminar burning speeds at low temperatures and high pressures.

The methods used to measure burning rates and flames speeds can be characterized as either constant pressure (Lui and McFalane 1983, Myers and Lefebvre 1986, Richards et al. 1989, Sher and Ozder 1992) or constant volume (Agrawal 1981, Clarke et al. 1995, Metghalchi and Keck 1982, Metghalchi and Keck 1980). Constant pressure methods, such as those employing flat flame burners, are limited to a relatively narrow range of temperatures and are most useful for obtaining data at atmospheric pressure. The principal disadvantages of the constant pressure methods are that they require significant corrections for flame geometry and conductive heat loss to the burner. Recently an effort has been made to measure the heat loss to the burner (Bosschaart and Goey 2003) and calculate the adiabatic burning speed, but this could only be done at atmospheric pressure and room temperature.

Constant volume methods, such as those employing spherical combustion chambers, cover a much wider range of temperatures and pressures and provide a range of data along an isentrope in a single experimental run. In addition, corrections for flame geometry or heat loss are generally quite small. Spherical chambers have been used by a number of

* Corresponding Author

investigators (Metghalchi and Keck 1980, Metghalchi and Keck 1982, Daly et al. 2001) to measure burning speeds for a wide range of fuels, equivalence ratios, diluent concentrations, pressures and temperatures. Flame instabilities such as cracking, wrinkling and buoyant rise have been observed by many researchers and have subtle effects (Daly et al. 2001, Gu et al. 2000, Aung et al. 1997).

In the current study, burning speeds have been calculated for methane-oxidizer-diluent (86 % N₂ and 14 % CO₂) mixtures for equivalence ratios of 0.8, 1.0 and 1.2 over the pressure range 1-50 atm and unburned gas temperature range 298-500 K. The pressure rise due to combustion in a constant volume spherical chamber was recorded and a thermodynamic analysis of the pressure time record was used to calculate the burning speeds. The flame structure was investigated using a cylindrical chamber with end windows. Buoyancy and instabilities in the flame structure were observed in this vessel. The determined values of the burning speeds from pressure rise have been compared to calculations made using the PREMIX flame speed code (Kee et al. 1985) with GRI-Mech 3.0 mechanism (Smith et al.). As expected, the agreement is good for high-temperature, low-pressure conditions. However for low temperature, high pressure conditions, the kinetic based calculated burning speeds are significantly higher than the measured values.

The significance of this thermodynamic model and this approach is that burning speeds of any fuel oxidizer mixture can be determined easily, while use of chemical kinetics requires knowledge of over 1000 reaction rate constants and high computation time for heavy hydrocarbons.

2. Experimental Facilities

The experiments were made in both a spherical and a cylindrical combustion chamber (Parsinejad et al. 2006 and Rahim et al. 2002). The spherical chamber consists of two hemispheric heads bolted together to make a 15.4 cm inner diameter sphere. The chamber was designed to withstand pressures up to 425 atm and is fitted with ports for spark electrodes, diagnostic probes, and for filling and evacuating. A thermocouple inserted through one of the chamber ports was used to check the initial temperature of the gas inside the chamber. A Kistler 603B1 piezo-electric pressure transducer with a Kistler 5010B charge amplifier was used to obtain dynamic pressure vs. time records from which the burning rate was determined. Ionization probes mounted flush with the wall at the top and bottom of the chambers were used to

measure the arrival time of the flame at the wall and check for spherical symmetry and buoyant rise.

The companion cylindrical chamber has a diameter and length equal to 13.3 cm, which makes its volume equal to that of the spherical chamber. This chamber was designed to operate over the same pressure and temperature range as the spherical chamber and is equipped with similar access ports. The primary purpose of this facility is to permit optical observation of the flame shape and structure under conditions as close as possible to those in the spherical chamber. Also, the initial pressure rise and flame development are identical in both chambers. A high speed CCD digital video camera is used to obtain shadowgraphs of the flame at speeds up to 8000 frames/second.

The gas handling system consists of a vacuum pump for evacuating the system and a valve manifold connected to gas cylinders for preparation of the fuel/oxidizer/diluent mixtures. Partial pressures of the fuel mixtures were measured using Kulite strain gauge pressure transducers in the 0-15 atm range. Two spark plugs with extended 2 mm diameter electrodes were used to ignite the mixture at the center of the chambers. An electronic ignition system controlled by the data acquisition program provides the spark.

The data acquisition system consists of a Data Translations 16 bit data acquisition card, which records the pressure change during combustion at a rate of 250 kHz. The analog to digital converter card receives the pressure signal from the charge amplifier and the signals from the ionization probes. All signals are recorded by a personal computer and an output data file is automatically generated. The output data file contains information about the partial pressures and initial temperature of all the gases used: fuel, oxygen and diluent. An oscilloscope is used to monitor the ignition signal and the outputs of the ionization probes and the pressure transducer in real time to insure that the various sensors are working and that the system has fired properly.

After the chamber is filled with the proper mixture, several minutes are allowed before the mixture is ignited. This is sufficient to permit any turbulence inside the vessel to decay. At least three runs at each initial condition were made to provide a good statistical sample. Based on a statistical analysis, it was found that three runs are enough to achieve a 95% confidence level.

3. Thermodynamic Model

The thermodynamic model used to calculate the burning speed from the pressure rise is based

on one previously developed by Metghalchi and Keck (1982 and 1980) modified to include the effects of temperature gradients in the burned gas, conduction energy losses to electrodes, radiation energy transfer from burned gases to vessel walls and inclusion of a flame preheat zone. It is assumed that gases in the combustion chamber can be divided into burned and unburned regions separated by a reaction layer of zero thickness as shown schematically in Figure 1. It is further assumed that: the burned and unburned gases are ideal, the burned gas is in chemical equilibrium, the unburned gas composition is frozen, the pressure throughout the chamber is uniform, and compression of both burned and unburned gases is isentropic. For the conditions of interest in the present work, all these assumptions have been validated by numerous experiments in constant volume chambers and internal combustion engines carried out over the past several decades.

3.1. Burned Gas Mass Fraction and Temperature

For spherical flames, the temperature distribution of the gases in the combustion chamber and the burned gas mass fraction can be determined from the measured pressure using the equations for conservation of mass and energy together with the ideal gas equation of state

$$pv = RT \quad (1)$$

where p is the pressure, v is the specific volume, R is the specific gas constant and T is the temperature.

The mass conservation equation is

$$m = m_b + m_u = p_i(V_c - V_e)RT_i \quad (2)$$

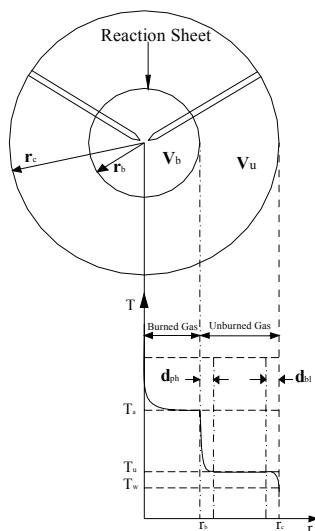


Figure 1. Schematic of the combustion chamber showing the flame geometry and the assumed radial temperature profile.

where m is the mass of gas in the combustion chamber, m_b is the burned gas mass, m_u is the unburned gas mass, V_c is the volume of the combustion chamber, V_e is the electrode volume, and the subscript i denotes initial conditions. The total volume of the gas in the combustion chamber is

$$V_c - V_e = V_b + V_u \quad (3)$$

where

$$V_b = \int_0^{m_b} v dm = \int_0^{m_b} v_{bs} dm - V_{eb} \quad (4)$$

V_b is the volume of the burned gas, v_{bs} is the specific volume of isentropically compressed burned gas,

$$V_{eb} = \int_0^{m_b} (v_{bs} - v) dm \quad (5)$$

V_{eb} is the displacement volume of the electrode boundary layers,

$$V_u = \int_{m_b}^m v dm = m(1 - x_b)v_{us} - V_{wb} - V_{ph} \quad (6)$$

V_u is the volume of the unburned gas, $x_b = m_b/m$ is the burned gas mass fraction, v_{us} is the specific volume of isentropically compressed unburned gas,

$$V_{wb} = \int_{wb} (v_{us} - v) dm \quad (7)$$

V_{wb} is the displacement volume of the wall boundary layer,

$$V_{ph} = \int_{ph} (v_{us} - v) dm \quad (8)$$

V_{ph} is the displacement volume of the preheat zone ahead of the reaction layer.

The energy conservation equation is

$$E - Q_w - Q_e - Q_r = E_b + E_u \quad (9)$$

where E is the initial energy of the unburned gas, Q_w is the conduction energy loss to the wall, Q_e is the conduction energy loss to the electrodes, Q_r is the energy loss due to radiation from the burned gas,

$$E_b = \int_0^{m_b} e dm = \int_0^{m_b} e_{bs} dm - E_{eb} \quad (10)$$

E_b is the energy of the burned gas, e_{bs} is the specific energy of isentropically compressed burned gas,

$$E_{eb} = \int_0^{m_b} (e_{bs} - e) dm \quad (11)$$

E_{eb} is the energy defect of the electrode boundary layer,

$$E_u = \int_{m_b}^m e dm = m(1 - x_b)e_{us} - E_{wb} - E_{ph} \quad (12)$$

E_u is the energy of the unburned gas, e_{us} is the specific energy of isentropically compressed unburned gas,

$$E_{wb} = \int_{wb} (e_{us} - e) dm \quad (13)$$

E_{wb} is the energy defect of the wall boundary,

$$E_{ph} = \int_{ph} (e_{us} - e) dm \quad (14)$$

E_{ph} is the energy defect of the preheat layer. Using the perfect gas relation

$$e - hf = pv / (\gamma - 1) \quad (15)$$

where h_f is the specific enthalpy of formation of the gas at zero degrees Kelvin and $\gamma = c_p / c_v$ is the ratio of the constant pressure and constant volume specific heats, and assuming constant specific heats for the gases in the boundary layers and the preheat zone, the integrals in Eqs. 11, 13 and 14 may be evaluated approximately to give

$$E_{eb} = p \int_{eb} (v_{bs} - v) dm / (\gamma_b - 1) = pV_{eb} / (\gamma_b - 1) \quad (16)$$

$$E_{wb} = p \int_{wb} (v_{us} - v) dm / (\gamma_u - 1) = pV_{wb} / (\gamma_u - 1) \quad (17)$$

$$E_{ph} = p \int_{ph} (v_{us} - v) dm / (\gamma_u - 1) = pV_{ph} / (\gamma_u - 1) \quad (18)$$

A relationship between the wall heat transfer and the displacement volume for a gas subject to a time dependent pressure has been derived by Keck (1981). In the case of rapidly increasing pressure such as that occurring during constant volume combustion, the terms representing compression work on the boundary layer may be neglected and resulting equations are

$$Q_e = pV_{eb} / (\gamma_b - 1) = E_{eb} \quad (19)$$

$$Q_w = pV_{wb} / (\gamma_u - 1) = E_{wb} \quad (20)$$

in which we have used Eqs. 16 and 17. Note that, to this approximation, the heat loss to the wall exactly equals the energy defect in the boundary layer. Substituting the relation $dm = \rho dV$ into Eqs. 5, 7 and 8 we obtain

$$V_{eb} = 2\pi r_e r_b \delta_{eb} \quad (21)$$

$$V_{wb} = 4\pi r_c^2 \delta_{wb} \quad (22)$$

$$V_{ph} = 4\pi r_b^2 \delta_{ph} \quad (23)$$

where r_e is the radius of the electrodes, r_b is the radius of the burned gas, r_c is the radius of the combustion chamber,

$$\delta_{eb} = \int_0^{r_b} \int_0^\infty (\rho(r, \eta) / \rho_{bs} - 1) d\eta dr / r_b \quad (24)$$

δ_{eb} is the displacement thickness of the electrode boundary layer in which η is the radial distance from the electrode,

$$\delta_{wb} = \int_{wb} (\rho(r) / \rho_{us} - 1) dr \quad (25)$$

δ_{wb} is the displacement thickness of the wall boundary layer, and

$$\delta_{ph} = \int_{ph} (\rho(r) / \rho_{us} - 1) dr \quad (26)$$

δ_{ph} is the displacement thickness of the preheat zone. Using the approximation

$$\int_{eb} (\rho(\eta, r) / \rho_{bs} - 1) d\eta = (\alpha_b (r_b - r) / \dot{r}_b)^{1/2} (T_b / T_w - 1) \quad (27)$$

Eq. 24 can be integrated over r to give

$$\delta_{eb} = (2/3) (\alpha_b r_b / \dot{r}_b)^{1/2} (T_b / T_w - 1) \quad (28)$$

where α_b is the thermal diffusivity of the burned gas, T_w is the wall temperature, and T_b is the burned gas temperature.

The wall boundary layer displacement thickness can be calculated using the expression derived by Keck (1981).

$$\delta_{wb} = \left(\frac{\alpha_u \tau}{\pi} \right)^{1/2} z^{-1/\gamma} \int_0^{\tilde{z}} (z' - z'^{1/\gamma}) \left(\int_{z'}^{\tilde{z}} z'' dz'' \right)^{-1/2} dz' \quad (29)$$

where α_u is the thermal diffusivity of the unburned gas, τ is a characteristic burning time, $y = t/\tau$ is the dimensionless time, and $z = p/p_i$ is the dimensionless pressure. For combustion in closed chambers, the dimensionless pressure can be approximated by

$$z = 1 + y^3 \quad (30)$$

Substituting this expression in Eq. 29 we obtain

$$\delta_{wb} \approx (\alpha_u t / \pi)^{1/2} (p_i / p)^{1/2} \left((p / p_i)^{(1-1/\gamma_u)} - 1 \right) \quad (31)$$

The displacement thickness of the preheat zone has been evaluated assuming an exponential temperature profile

$$T/T_u \approx 1 + (T_b/T_u - 1) \exp(-\alpha_u (r - r_b) / \dot{r}_b) = \rho_s / \rho(r) \quad (32)$$

Substituting Eq. 32 into Eq. 26 we obtain

$$\delta_{ph} = - \int_{ph} ((T_b/T_u - 1)^{-1} \exp(r - r_b) \dot{r}_b / \alpha_u + 1)^{-1} (r/r_b)^2 dr \quad (33)$$

$$r \gg \alpha_u / \dot{r}_b,$$

Eq. 33 can be integrated approximately to give

$$\delta_{ph} \approx -(\alpha_u / \dot{r}_b)(T_b/T_u - 1) \ln(T_b/T_u) \quad (34)$$

Note that the displacement thickness of the preheat zone is negative while those of the thermal boundary layers are positive.

The radiation energy loss from the burned gas was calculated using

$$\dot{Q}_r = \int_0^t \dot{Q}_r dt' \quad (35)$$

where

$$\dot{Q}_r = \alpha_p V_b \sigma T_b^4 \quad (36)$$

is the radiation rate, α_p is the Planck mean absorption coefficient and σ is the Stefan-Boltzman constant.

Finally combining Eqs. 3, 4 and 6 gives

$$\int_0^{x_b} (v_{bs} - v_{us}) dx = v_i - v_{us} + (V_{eb} + V_{wb} + V_{ph})/m \quad (37)$$

and combining Eqs. 9, 10, 12 and 18-20 gives

$$\int_0^{x_b} (e_{bs} - e_{us}) dx = e_i - e_{us} + (pV_{ph}/(\gamma_u - 1) - \dot{Q}_r)/m \quad (38)$$

where $v_i = (V_c - V_e)/m$ and $e_i = E_i/m$ are the initial specific volume and energy of the unburned gas in the chamber.

Equations 37 and 38 contain the three unknowns p , $x_b(p)$, and $T_b(x_b)$. Given pressure, $p(t)$, as a function of time, they can be solved numerically using the method of shells to obtain the burned mass fraction, $x_b(t)$, as a function of time and the radial temperature distribution $T(r, t)$. The mass burning rate, $\dot{m}_b = m\dot{x}_b$, can be obtained by numerical differentiation of $x_b(t)$. The thermodynamic properties of the burned and unburned species used in the calculations were obtained from the JANAF Tables.

If the specific heats of the burned and unburned gases are assumed constant, Eq. 15 can be used to evaluate the integral in Eq. 38 and we obtain

$$p(v_{bs}/(\gamma_b - 1) - v_{us}/(\gamma_u - 1)) = h_{ub} + p(v_i - v_{us})/(\gamma_u - 1) + (pV_{ph}/(\gamma_u - 1) - \dot{Q}_r)/m \quad (39)$$

where $h_{ub} = h_{fu} - h_{fb}$ is the difference between the enthalpies of formation of the unburned and burned gas at zero degrees Kelvin.

3.2. Burning Speed, Flame Speed and Gas Speed

For closed flames, the burning speed may be defined

$$S_b = \dot{m}_b / \rho_u A_b \quad (40)$$

where A_b is the area of a sphere having a volume equal to that of the burned gas. This expression is valid for smooth, cracked, or wrinkled flames of any shape. For smooth spherical flames

$$\dot{m}_b = \dot{\rho}_b V_b + \rho_b A_b \dot{r}_b \quad (41)$$

where ρ_b is the average value of the burned gas density.

Differentiating the mass balance equation

$$m_b = m - \rho_u V_u = (\rho_u/\rho_b)\rho_b(V_c - V_e - V_b) \quad (42)$$

with respect to time and neglecting the small contribution from the derivative of ρ_u/ρ_b , we obtain

$$\dot{m}_b = (\rho_u/\rho_b)((V_c - V_e - V_b)\dot{\rho}_b - \rho_b A_b \dot{r}_b) \quad (43)$$

where

$$A_b = 4\pi r_b^2 - 2\pi r_e^2 \quad (44)$$

is area of the reaction zone, r_e is the electrode radius and V_b is given by the equation

$$V_b = (4/3)\pi r_b^3 - 2\pi r_e^2 r_b \quad (45)$$

Using Eq. 41 to eliminate $\dot{\rho}_b$ in Eq. 43, gives

$$S_f = \dot{r}_b = S_b(\rho_u/\rho_b - y_b(\rho_u/\rho_b - 1)) \quad (46)$$

where S_f is the flame speed and $y_b = V_b/(V_c - V_e)$ is the burned gas volume fraction. Note that for $y_b=0$, $S_f = (\rho_u/\rho_b)S_b$ and for $y_b=1$, $S_f = S_b$. The gas speed is defined by

$$u_g = S_f - S_b \quad (47)$$

Substituting Eq. 46 into Eq.47 we obtain

$$u_g = S_b(\rho_u/\rho_b - 1)(1 - y_b) \quad (48)$$

This completes the equations for the burning model.

4. Comparison of Results of Thermodynamic Model with Kinetics Model Predictions

For comparison with thermodynamic results, the burning speeds of steady laminar adiabatic one-dimensional pre-mixed methane/oxygen/diluents flames have been computed using the SANDIA PREMIX code (Kee et al. 1985), marketed by Reaction Design. A reaction mechanism involving 53 species and 325 elementary reactions was taken from GRI-Mech 3.0 (Smith et al.). This mechanism is optimized for burned gas temperatures from approximately 1000 to 2500 K, pressures from

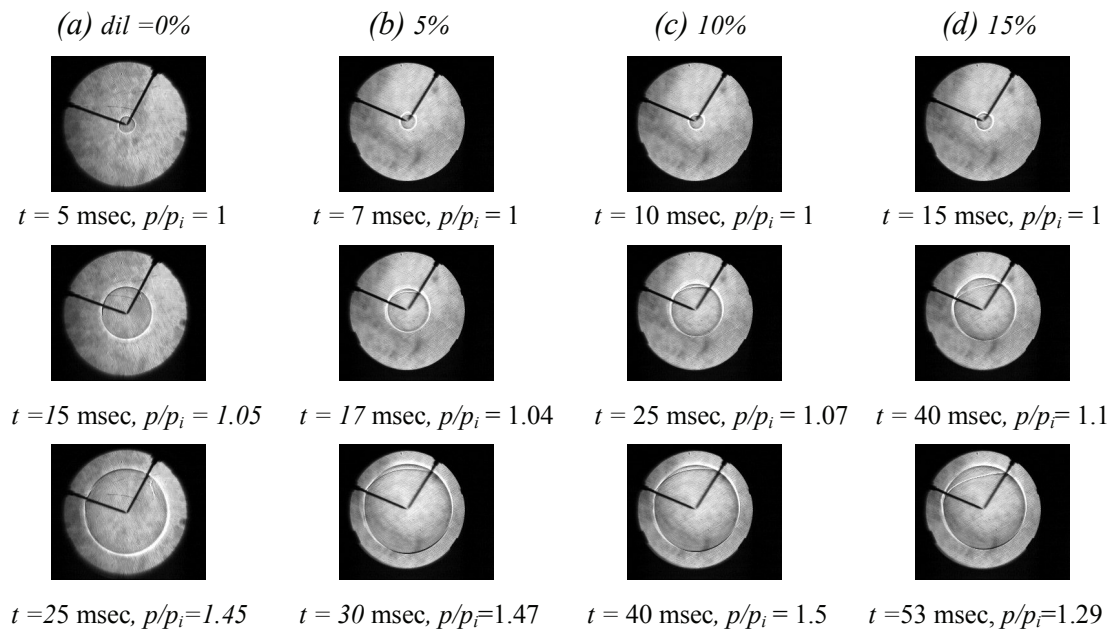


Figure 2. Shadowgraphs showing flame propagation in the cylindrical chamber for stoichiometric methane-oxidizer-diluent mixtures at several diluent fractions and $\phi=1.0$, $p_i=1.0$ atm, and $T_i=298$ K.

10 Torr to 10 atm, and equivalence ratios from 0.1 to 5 (Smith et al.). It was chosen for the calculations because it has been widely used for laminar flame speed calculations.

The comparisons were made for a wide range of conditions spanning both the high and low temperature regimes. The conditions under which significant cracking or wrinkling occurred were observed and are reported. A mixture of 86 % N_2 and 14 % CO_2 is used for the extra diluent to simulate the molar mass and specific heat of the exhaust gas in internal combustion engines.

Observations of the flame structure were carried out in the cylindrical chamber. Although this vessel is not spherical, the flame propagates spherically over 90 percent of the distance to the wall.

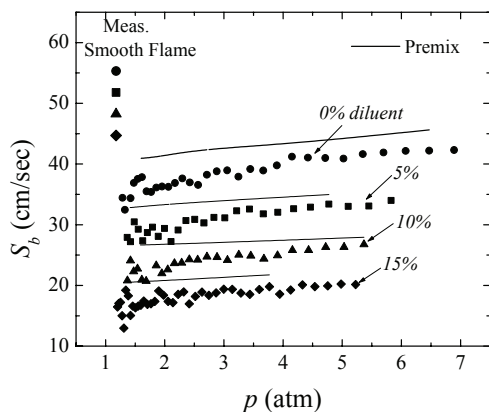


Figure 3. Comparison of measured burning speeds along isentropes with PREMIX calculations for the same conditions as Fig. 2.

Shadowgraph photographs of flame fronts for stoichiometric methane-oxidizer-diluent mixtures with initial pressure and temperature of 1.0 atm and 298 K are shown in Figure 2 for 0-15% diluent. In these photographs, the final pressure is approximately 5 times the initial pressure. It can be seen that at all conditions, the flame front is smooth and spherical except for a single crack near the top, extending between the electrodes. This suggests that cracking may be caused at least in part by an interaction between the flame front and the electrodes.

The corresponding burning speeds along isentropes computed from the pressure rise in the spherical chamber are shown by the solid points in Figure 3. All the calculated values based on measurement are for smooth flames with large radii and therefore represent laminar adiabatic burning speeds. The solid lines show values calculated using PREMIX with GRI-Mech 3.0 kinetics. It can be seen that adding diluent decreases both the burning speed and the final pressure achieved in the vessel. The dependence of the flame speed on percentage of diluent is reproduced reasonable well by the PREMIX calculations but the absolute values are roughly 10-15% higher than the thermodynamic results for all conditions.

Shadowgraph photographs of flame fronts for stoichiometric methane-oxidizer-diluent mixtures with initial pressure and temperature of 5 atm and 298 K are shown in Figure 4 for 0-15% diluent. For the mixtures with zero diluent shown in part a, cracking can be seen for $p/p_i=1.03$ while for $p/p_i=1.4$, the flame is

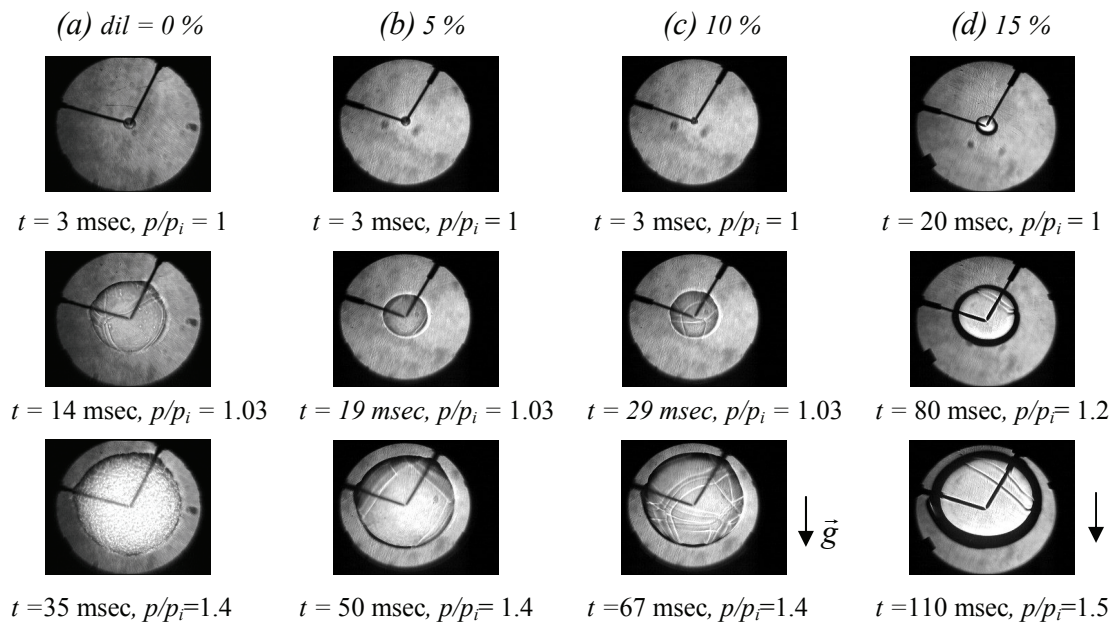


Figure 4. Shadowgraphs showing flame propagation in the cylindrical chamber for stoichiometric methane-oxidizer-diluent mixtures at several diluent fractions and $\phi=1.0$, $p_i=5.0$ atm, and $T_i=298$ K.

cellular. Parts b-d show that adding diluent results in flames that are cracked but not cellular. As the percentage of diluent increases the degree of cracking decreases indicating a more stable flame front. For 15% diluent, buoyant rise of the very slow flame can be observed.

Figure 5 shows the measured burning speeds corresponding to Fig 4. Solid symbols refer to cracked flames and open symbols to cellular flames. The results of PREMIX are shown by the solid lines. Again as the percentage of diluents increases the burning speed decreases. It can be seen that the agreement between thermodynamic results and PREMIX calculations is reasonably good for cracked flames with 0-15% diluent. However for cellular flames with zero diluent, they disagree. This may be due to an increased effective burning area for cellular flames.

Shadowgraphs of lean methane-oxidizer-diluent flames with equivalence ratio $\phi=0.8$ and

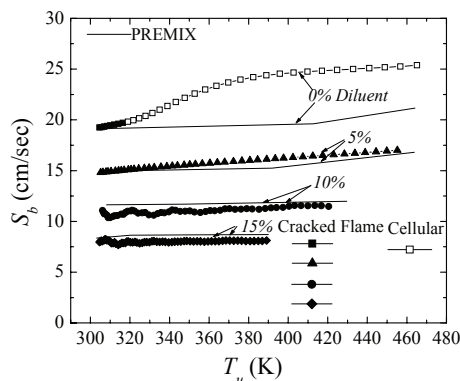


Figure 5. Comparison of measured burning speeds along isentropes with PREMIX calculations for the same conditions as Fig. 4.

initial pressure and temperature of 5 atm. and 298 K are shown in Fig. 6 for 0-10% diluent. All the flames in this figure show some cracks. Parts a-b show that for 0-5% diluent, cells appear on the flame surface at the highest pressure ratios. Part c shows buoyant rise and distortion of the slow flames with 10% diluent. Ionization probes mounted flush with the wall at the top and bottom of the chamber were used to check the degree of distortion and buoyant rise rate. This shows that distortion of the flame front can be quite large before the expected increase in flame area becomes observable.

Figure 7 shows a comparison of the thermodynamic results with PREMIX calculations for the lean flames. Cracked flames are shown by solid symbols and cellular flames by hollow symbols. PREMIX calculations are shown by solid lines. As previously seen in Fig 5, the burning speed calculated from the thermodynamic model for the cellular flames having 0% and 5% diluent are higher than those calculated using PREMIX. For cracked flames at 0-5% the agreement is very well. As the diluent is increased to 10%, the results of the thermodynamic model drop below the PREMIX values.

Shadowgraphs of flame propagation for rich methane-oxidizer-diluent mixtures with equivalence ratio $\phi = 1.2$ and initial pressure and temperature of 5 atm and 298 K are shown in Figure 8 for 0-10% diluent. For all diluent fractions, the flames are smooth with very few cracks but some distortion and buoyant rise apparent for slow flames.

The calculated burning speeds of these

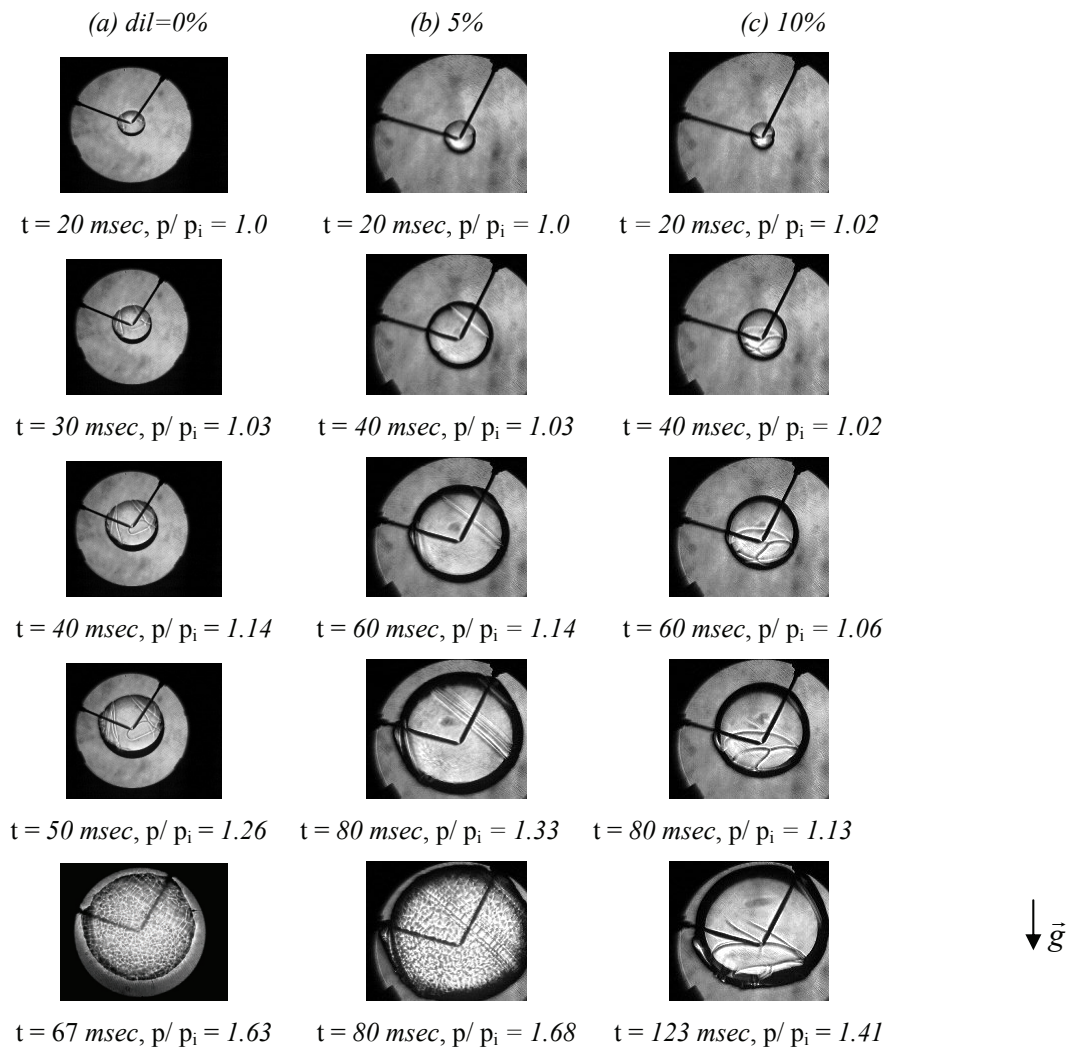


Figure 6. Shadowgraphs showing flame propagation in the cylindrical chamber for lean methane-oxidizer-diluent mixtures at several diluent fractions and $\phi=0.8$, $p_i=5.0$ atm, and $T_i=298$ K

flames are compared with PREMIX results in Figure 9. It can be seen that the calculated burning speeds are significantly lower than the PREMIX values for all diluent fractions. Since these flames are smooth, this indicates a failure

of the GRI-Mech 3.0 kinetics as anticipated for high pressure rich flames. Other investigators (Kwon et al. 2002 and Rozenchan et al. 2001) have also observed similar discrepancies between measured burning speeds and calculations using GRI-Mech 3.0 kinetics at high pressures.

5. Summary and Conclusions

Burning speeds for methane-oxidizer-diluent flames over a wide range of pressures, temperatures, equivalence ratios, and diluent fractions have been determined using a thermodynamic model from pressure measurements made in a spherical combustion chamber. Shadowgraphs were taken through end windows in a cylindrical chamber of the same volume as the spherical chamber to determine the shape and structure of the flames for which burning speeds were measured. Both spherical and distorted flames having smooth, cracked and cellular fronts were observed. For very slow flames, buoyant rise was also observed. For comparison with the measurements, flame

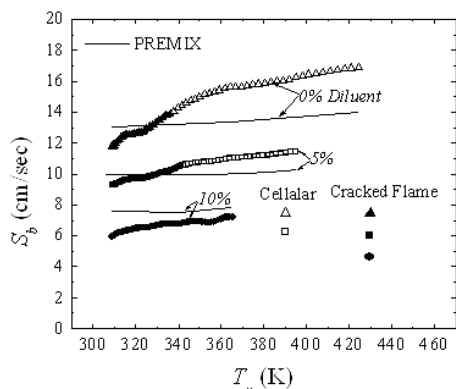


Figure 7. Comparison of measured burning speeds along isentropes with PREMIX calculations for the same conditions as Fig. 6

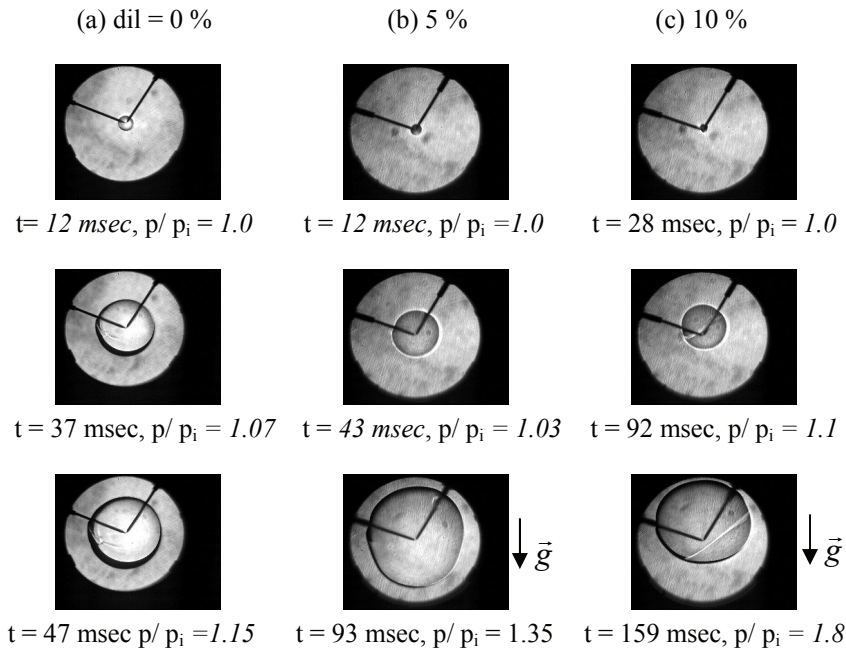


Figure 8. Shadowgraphs showing flame propagation in the cylindrical chamber for rich methane-oxidizer-diluent mixtures at several diluent fractions and $\phi=1.2$, $p_i=5.0$ atm, and $T_i=298$ K.

speeds were calculated using the PREMIX code with GRI-Mech 3.0 kinetics. The following conclusions were drawn:

1. Burning speeds of stoichiometric methane-oxidizer-diluent mixtures at initial pressures and temperatures of 1.0 atm and 298 K and 0-15% diluent are in reasonable agreement with values calculated from the PREMIX code using GRI-Mech 3.0 kinetics. Under these conditions all the flames observed were smooth and spherical.

2. For initial pressures and temperatures of 5.0 atm and 298 K and 0-15% diluent, stoichiometric and lean methane-oxidizer-diluent flames were cracked at low pressures and high diluent fractions and cellular at high pressures

and low diluent fractions. Burning speeds for cracked flames agree reasonably well with PREMIX values for cellular but are higher than PREMIX values for cellular flames suggesting that cellularity may increase the burning speed.

3. For rich methane-oxidizer-diluent mixtures at initial pressures and temperatures of 5.0 atm and 298 K, and 0-10% diluent, all the flames observed were smooth but the calculated burning speeds were significantly lower than those predicted by PREMIX code.

4. Further work is needed to determine more precisely the conditions under which cracking and cellularity occur and whether the observed discrepancies between the calculated burning speeds and PREMIX results are due to cellularity or a failure of the GRI-Mech 3.0 kinetics.

5. The structure of developed thermodynamic model is independent of chemical reactions which occur in the system, so the calculations are remarkably simplified both from mathematical and computation time perspective.

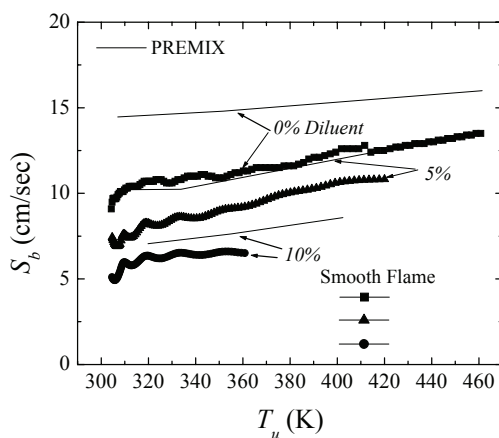


Figure 9. Comparison of measured burning speeds along isentropes with PREMIX calculations for the same conditions as Fig. 8.

Acknowledgements

This research was partially supported by the Army Research Office, Grant No. W911NF-05-1-0051, under technical monitoring of Dr. Ralph Anthenien. The authors would like to thank Professor James C. Keck, MIT, for helpful scientific discussions. Mr. Craig Hoffstein, and Ms. Lina Song are appreciated for their help in developing this manuscript.

Nomenclature

A = area
E = energy
 c_p = constant pressure specific heat
 c_v = constant volume specific heat
e = specific energy
 h_f = specific enthalpy of formation
m = mass
p = pressure
Q = heat loss
r = radius
R = specific gas constant
 S_b = mass burning speed

Greek Letters

α = thermal diffusivity
 α_p = Planck mean absorption coefficient
 δ = boundary displacement thickness
 γ = ratio of constant pressure and constant volume specific heats
 η = radial distance from electrode
 ρ = density
 σ = Stefan-Boltzman constant
 τ = characteristic burning time

Subscripts

b = burned gas
e = electrode
i = initial conditions
r = radiation
u = unburned gas
w = wall
eb = electrode boundary layer
wb = wall boundary layer
ph = preheat zone
bs = isentropically compressed burned gas
us = isentropically compressed unburned gas

References

Agrawal, D., 1981 *Combustion and Flame*, 42, pp. 243-252.
Aung, K.T., Hassan, M.I., and Faeth, G.M., 1997, *Combustion and Flame*, 109, pp. 361-384.
Bosschaart, K.J., and de Goey, L.P.H., 2003 *Combustion and Flame*, 132, pp. 170-180.
Clarke, A., Stone, R., and Beckwith, P., 1995 *J. of the Institute of Energy*, 68, pp. 130-136.
Daly, C.A., Simmie, J.M., Wurmel, J., Djebaili, N., and Paillard, C., 2001, *Combustion and Flame*, 125 pp. 1329-1340.

Davis, S.G., Law, C.K., and Wang, H., 1998, *Twenty-Seventh Symposium (international) on Combustion*, Combustion Institute, Boulder, CO, pp 305-312.

Gu, X.J., Haq, M.Z., Lawes, M., and Wooley, R., 2000, *Combustion and Flame*, 121, pp. 41-58.

Habik, S., El-Sherif, S.A., Cho, P., and Abata, D.L., 1999, *Comb Sc and Tech*, 148, pp. 93-133.

Hunter, T.B., Wang, H., Litzinger, T.A., and Frenklach, M., 1994, *Combustion and Flame*, 97 pp. 201-224.

JANAF Thermochemical Tables, 1986 Third Edition ed.: Am Ch. Institute, American Institute of Physics, National Bureau of Standards.

Keck, J.C., 1981, *Letters in Heat and Mass Transfer*, 8 (4), pp. 313-319.

Kee, R.J., Gracar, J.F., Smooke, M.D., and Miller, J.A., 1985, Sandia Report.

Kwon, O.C., Rozenchan, G., and Law, C.K., *Twenty-ninth International Symposium on Combustion*, Sapporo, Japan, 2002, July 21 - 26, Proc of the Comb Inst, Vol. 29, p 1775-1783.

Lui, D., and McFarlane, R., 1983, *Combustion and Flame*, 49, pp. 59-71.

Metghalchi, M. and Keck, J.C., 1980 *Combustion and Flame*, 38, pp. 143-154.

Metghalchi, M. and Keck, J.C., 1982 *Combustion and Flame*, 48, pp. 191-210.

Myers, G., and Lefebvre, A., 1986 *Combustion and Flame*, 66, pp. 193-210.

Parsinejad, F., Arcari, C., and Metghalchi, H., 2006, *Combustion Science and Technology*, Volume 178, Number 5, pp. 975-1000(26).

Rahim, F., Elia, M., Ulinski, M., and Metghalchi, M., 2002 *International Journal of Engine Research*, 3 (2) pp. 81-92.

Richards, G., Sojka, P., and Lefebvre, A., 1989 *Transaction of the ASME gas turbine conference*, pp 84-89.

Rozenchan, D., Tse, S.D., Zhu, D.L., and Law, C.K., 2001, *39th Aerospace Science Meeting and Exhibit*, AIAA 2001-1080, Reno, NV.

Sher, E., and Ozder, N., 1992, *Combustion and Flame*, 89, pp. 214-220.

Smith, G.P., Golden, D.M., Frenklach, M., Moriarty, N.W., Eiteneer, B., Goldenberg, M., Bowman, C.T., Hanson, R.K., Song, S., Gardiner Jr., W.C., Lissianski, V.V., and Qin, Z., http://www.me.berkeley.edu/gri_mech/.

Warnatz, J., 1984, *Twentieth Symposium (International) on Combustion*, The Combustion Institute, University of Michigan, USA, pp 845-856.